Title: The Adjuvant Effects of Amphipathic Helical Peptides

Jyun-Hong Lyu[1], Gunn-Guang Liou[2,3], May Wang[1], Ming-Chung Kan[1,4]

1. Vaxsia Biomedical Inc. 11503 Taipei, Taiwan
2. Institute of Biological Chemistry, Academia Sinica, 11529 Taipei, Taiwan
3. Office of Research and Development, College of Medicine, National Taiwan University, 10051 Taipei, Taiwan
4. Corresponding author

Abstract

Subunit vaccines are the focus of research in developing new vaccines against infectious diseases. Due to the low immunogenicity of recombinant proteins, adjuvants are required for the activation of humoral and cellular immunity against a protein antigen. In this study, we reported the identification of a novel pathway that can activate humoral immunity against a recombinant protein without inducing inflammatory responses. By fusing an amphipathic helical peptide to GFP, one can increases the immunogenicity of GFP by up to 1000 fold. This enhancement was correlated with the ability of amphipathic helical peptides to bind to cell membranes and cause lysosomal membrane permeabilization. We showed evidence that the amphipathic helical peptide may induce the delivery of antigen across the lysosomal membrane into cytosol. Amphipathic helical peptide fusion provided a new pathway for stimulating immune responses against recombinant proteins.

Introduction

The challenge of developing a subunit vaccine focuses on two aspects: first, finding the right antigen that may serve as a countertarget for the host immune system; and second, enhancing the specific host immune responses through various

30 mechanisms to a level that can counter the pathogen but will not cause harm to the
31 host. The antigens for subunit vaccines come from various components of the
32 pathogen: polysaccharides, viral proteins that mediate infection, and toxins that
33 cause host morbidity or mortality. These antigen candidates are poor at activating
34 the host immune system and often require the addition of an adjuvant. The adjuvant,
35 according to the FDA, is a compound that is added to or used in conjunction with the
36 vaccine antigen to augment, potentiate, or target a specific immune response to the
37 antigen [1]. The adjuvant may be presented to the immune system in different forms
38 and activate immune responses through various pathways.

39 The amphipathic peptide is characterized by the propensity of a peptide to
40 form both hydrophilic and hydrophobic surfaces and mediates the interactions
41 between protein and membrane [2]. The M2 amphipathic helical (M2AH) peptide is
42 the membrane anchor of the type A influenza virus proton pump [3]. M2 proteins
43 form a cross-membrane tetramer, transporting protons needed for endosome
44 acidification and viral particle escape [3]. The M2AH resides on the cytoplasmic
45 surface of the host membrane and induces membrane curvature and scission in a
46 cholesterol concentration-dependent manner [4-6]. In a phospholipid bilayer
47 containing cholesterol, the binding of M2AH induces membrane pit formation and a
48 weakening of the lipid bilayer [7]. An M2AH variant is able to induce cholesterol-
49 dependent membrane leakage or membrane lysis [4]. In this study, we have
50 identified several amphipathic helical peptides that stimulated strong humoral
51 immunity when they were fused with a model antigen, green fluorescent protein
52 (GFP) and used in immunization.
53
54 Result
55 To test the effects of an amphipathic helical peptide on the immunogenicity of a
56 recombinant protein, we fused a peptide (AH2) from the M2 protein of a type A

57 influenza virus strain, A/TW/3355/97(H1N1) to green fluorescent protein (GFP). The
58 fusion proteins were expressed and purified from *E. coli* strain BL21(DE3). The
59 purified fusion proteins were used for the immunization of BALB/c mice using a
60 prime and boost protocol. A variant of the AH2 peptide (AH2M3) that contains three
61 substitutions that disrupted the membrane binding activity of AH2 was used as a
62 negative control. After immunization, the anti-GFP IgG titer was followed for up to 6
63 months. Compared to His-GFP alone, the fusion protein contains a functional
64 amphipathic helical peptide is able to stimulate a higher level of anti-GFP IgG titer
65 (Figure 1B), whereas the membrane binding defective mutant, AH2M3 (Figure 1C),
66 was unable to activate humoral immunity against GFP. The IgG subtype of the sera
67 collected was then determined using subtype-specific secondary antibodies. The
68 result showed the titer of IgG1 is significantly higher than either IgG2a or IgG2b, an
69 indication that the immune response is tilted toward the Th2 type (Figure 1D).
70 One potential explanation of amphipathic helical peptide-mediated immunity
71 boosting is by activating Toll-Like Receptor (TLR) pathways, the major mechanism
72 for boosting recombinant protein antigenicity by adjuvants. To test this hypothesis,
73 we collected the mouse plasma 2 hours after intramuscular injection of either PBS,
74 GFP, AH2-GFP, or TLR5 ligand, flagellin, and examined the expression of
75 inflammatory cytokines, IL-6 and MCP-1. IL-6 and MCP-1 are cytokines that are
76 secreted by macrophages after activation of TLR pathways by invading pathogens or
77 adjuvants. The flagellin is the structural component of bacterial flagellum that
78 controls microbe movement and is the ligand for TLR5. The results showed a dose-
79 dependent induction of IL-6 and MCP-1 expression by injected recombinant flagellin
80 (Figure 2A, 2B). But not when the mice were injected with His-GFP or AH2-GFP
81 recombinant proteins. These results suggest that the activation of humoral
82 immunity by AH2-GFP is independent from the TLR signaling pathways; instead, the
83 activity of AH2-GFP is correlated with its ability to bind plasma membrane.
84 To trace the transportation of AH2-GFP fusion protein after binding to the plasma
85 membrane, we incubated purified AH2-GFP fusion protein with cultured MDCK cells
86 for four hours and evaluated whether AH2-GFP will be endocytosed into the cell.
87 The confocal images showed the endocytosed AH2-GFP in a vesicle-like structure

88 (Figure 3A). To trace the transportation of endocytosed AH2-GFP, we conjugated the
89 AH2 peptide onto the surface of a gold nanoparticle (G-NP) and used a transmission
90 electronic microscope to trace the tansportation of peptide conjugated AH2-G-NP.
91 The cultured cell was either incubated with AH2-G-NP for 4 hours (Figure 3B-C) or
92 4+20 hours (Figure 3D-E) before being washed and processed for TEM imaging. The
93 results showed that four hours after AH2-G-NP binding to the plasma membrane,
94 AH2-G-NP containing membrane (marked by arrows) was transported to the
95 multivesicular body (MVB), an organelle for membrane protein sorting, or the
96 lysosome (membrane rich and electron dense vesicle, labled L). In 4+20 hours post
97 incubation, many AH2-G-NPs were observed in enlarged lysosomes (L) and many
98 within permeabilized membranes (PL). Some of the enlarged lysosomes were
99 shown with broken membranes, possibly due to the AH2-G-NP and some aggregated
100 AH2-G-NP can be observed being released into the cytoplasm (marked by arrow
101 heads). These results suggest the fusion of GFP with an amphipathic helical peptide
102 not only mediates the binding of fusion protein onto the plasma membrane but also
103 the transport and delivery of fusion protein into the cytoplasm through a
104 permeabilized lysosome.
105 Amphipathic helical peptides play multiple roles in the protein-membrane
106 interactions, including membrane anchorage, inducing membrane curvature, and
107 membrane lysis [2,8]. To evaluate whether the AH2 peptide possessed membrane
108 lysis activity as implicated in Figure 3C, the synthetic AH2, AH2M3, and Udorn
109 peptides in increasing concentrations were applied to cultured Madin-Darby canine
110 kidney (MDCK) cells. The positive control Udorn peptide, a M2 AH peptide that was
111 derived from the influenza strain A/Udorn/72, has been shown to induce membrane
112 leakage in an artificial liposome that contains low percentage of cholesterol in an in
113 vitro assay [4]. The effect of synthetic peptides on the viability of cultured MDCK
114 cells was determined by flow cytometry for cells undergoing apoptosis and the MTT
115 assay for cells with metabolic activity. The results suggested 20% of the MDCK cells
116 incubated with Udorn peptide became apoptotic at a peptide concentration of 10 μM
117 and the percentage of apoptotic cells increased with elevated peptide concentration

118 (figure 4A). This result is in agreement with a previous study from Lamb's group [4].
119 In contrast, the percentage of MDCK cells undergoing apoptosis when treated with
120 AH2 peptide concentrations up to 100 μM was not significantly different from those
121 treated with PBS. In the MTT assay, the mitochondrial dehydrogenase enzyme
122 activity of cells treated with Udorn peptide dropped significantly compared to cells
123 treated with AH2 peptide in all three peptide concentrations. Whereas the viabililty
124 of MDCK cells treated with AH2 peptide only became significantly different from the
125 PBS control when the peptide concentration reached 100 μM. These results suggest
126 the AH2-fusion protein has to reach 100 μM (3.5 mg/ml) to induce a minor
127 reduction in cell viability.
128 To test whether AH2-mediated activation of humoral immunity is a particular
129 phenomenum or a common feature of amphipathic helical peptides, we replaced the
130 AH2 peptide with published AH peptides from either NSP1 of the Semliki Forest
131 virus (NSP1), G-protein coupled protein kinase 5 (GRK5), or the fusion peptide of
132 hemagglutinin (HAfp23). These fusion proteins were expressed and purified under
133 the same conditions as AH2-GFP and were used for mouse immunization using a
134 two-dose protocol with a 14-day gap. The results showed all the fusion peptides
135 tested were able to boost the anti-GFP IgG titer by a magnitude about 1000 folds
136 after fusing to GFP. This increase in antibody titer against a recombinant protein is
137 significant when compared to the adjuvants that have been used to boost the
138 antigenicity of subunit vaccines. The use of alum salt increased the anti-GFP IgG
139 titer by 10 fold and the TLR4 ligand MPLA also had similar activities but not as
140 significant as the GRK5 peptide fusion (Figure 5B).
141
142 Discussion
143
144 The study results indicate that the AH peptide fusion enhanced the antibody
145 production against the model antigen, GFP. This increase is significant since the
146 comparison with known adjuvants suggests AH peptide fusion is more effective in
147 stimulating antibody production. Adjuvant that activates Th1 type immune

148 responses activates CD4+ T cells and IgG2a expression, whereas adjuvant that
149 activates the Th2 pathway induces IgG1 expression through CD8+ T cells. We have
150 not tested whether the AH peptide fusion also activates cellular immunity against
151 GFP-expressing cells, but the IgG subclass indicates a balanced activation of both T
152 helper type 1 (Th1) and Th2 pathways.
153 In our results, the binding of AH2-G-NP caused permeabilization of the lysosome
154 membrane but not the plasma membrane. In an in vitro membrane binding study,
155 the M2AH peptide (the same Udorn peptide as in this study) induced membrane
156 leakage in a synthetic liposome when the liposome membrane contained a low
157 percentage cholesterol but not when the membrane contained a high percentage
158 cholesterol [4]. Since the distribution of cholesterol in mammalian cells is organelle
159 dependent, it is rich in the multivesicular body (MVB) and the plasma membrane
160 but low in the lysosome membrane [9], so it is likely that the AH2 peptide only
161 induced membrane leakage when sorted into the lysosome. Another study
162 suggested M2AH binds cholesterol through the aromatic side chains of F47 [5] and
163 the binding of M2AH weakens the lipid bilayer by introducing membrane pits [7]. So
164 the binding of the AH2 peptide likely introduces cholesterol depleted membrane
165 pits and causes lysosomal membrane leakage. This mechanism is similar to that of
166 QS-21, the main component of several clinically approved adjuvants, which induces
167 endocytosis and lysosome pore formation through binding to cholesterol [10]. Other
168 adjuvants that activate immunity through lysosomal leakage include alum salt
169 [11,12].
170 The AH2-GFP fusion protein immunization did not induce acute expression of IL-6
171 or MCP-1, two inflammatory cytokines. There are two potential explanations for this
172 result. First, as the QS-21 study suggested, the QS-21 effect on the NF-kB pathway
173 and its downstream effects, including IL-6 expression, is depend on lysosomal
174 maturation, which takes longer than TLR signaling. So the time points (2 hrs post
175 injection) used to determine cytokine level in this study may be too early to catch
176 the IL-6 expression induced by the lysosomal leakage and its downstream NF-κB
177 activation. One study worth mentioning was the delayed induction of IL-6 and other

178 inflammatory cytokines after immunization with alum-salt adjuvanted antigen [13].
179 Another potential explanation is the distinct pathways that leading to NF-kB
180 signaling and IgG antibody titer induction activated by QS-21 [10]. In this aspect, the
181 AH2 peptide plays a similar role as QS-21, or they share the same ability to
182 destabilize the lysosomal membrane. Applying QS-21 alone causes cell apoptosis, so
183 it is often formulated with cholesterol and phospholipids to reduce cytotoxicity [14-
184 16]. But the formulation of a protein-based vaccine in an oil-in-water nanoemulsion
185 adjuvant may cause instability of the antigen when it is stored at ambient
186 temperature, and it required either lyophilization [17] or spray drying [18] after
187 adding excipients to achieve long-term thermostability. In comparison, protein
188 nanoparticles assembled by an amphipathic helical peptide are self-adjuvanted and
189 can be stored as ready-to-use doses at ambient temperature [19,20].
190 In this study, several known amphipathic helical peptides were used to evaluate
191 their effects on GFP antigenicity. The GRK5-AH is derived from the C-terminal AH
192 peptide of G protein-coupled protein kinase 5 (GRK5) [21]. Together with the N-
193 terminal helical basic peptide it anchors the GRK5 protein onto the plasma
194 membrane [22]. The NSP1-AH is adopted from the replicase of the Semliki forest
195 virus, nsP1 [23,24]. This peptide is conserved in replicase from all alphaviruses,
196 including Chikungunya virus [25]. The HAfp23-AH is the fusion peptide of
197 hemagglutinin from influenza virus that induces membrane curvature and fusion
198 through two tightly packed hairpin helices buried in the lipid bilayer [26]. There is
199 no similarity in peptide sequences among the four peptides presented in this study
200 or shared mechanism that can fully explain their activity in boosting antigenicity.
201 The common feature is the tendency to interact with phospholipid membranes
202 through their hydrophobic faces. One potential explanation comes from our recent
203 work [19]. When the Cys8 from a modified M2AH peptide, LYRRLE, was replaced by
204 serine, the substitution caused the destabilization and hydrolysis of protein
205 nanoparticles, and the particle size increased from 23 nm to 600 nm, suggesting the
206 particle was a loosely packed aggregation [19]. So the activity of AH peptides in
207 enhancing anti-GFP IgG may reside in their ability to form a random aggregation
208 after fusing with GFP. Other example of GFP fusion proteins forming aggregated

209 megastructures and gaining high antigenicity have been reported when GFP was
210 fused with the N-terminal domain of polyhedrin protein [27]. But the replacement of
211 GFP with known vaccine antigen in this megastructure is difficult because of the
212 interference with protein folding when proteins are packed closely.
213 Two synthetic peptides were reported to serve the role of an adjuvant. The Q-11
214 peptide self-assembled into an extended nanofibril structure that stimulated long-
215 lasting humoral and cellular immunity to the covalently fused peptide if proper
216 epitopes were provided [28-30]. The Q-11 peptide's activities depend on T cells and
217 MyD88, a typical signaling molecule that mediates innate immunity, but no
218 inflammatory responses were observed when immunizing with a Q-11-based
219 vaccine [29]. The other self-assembling peptide is coil-29, which forms an extended
220 spiral tube structure [31]. The coil-29 also shares similar activity with the Q-11, but
221 it has higher potency in inducing both types of immunity [32]. Interestingly, the coil-
222 29 peptide is predicted to be an amphipathic helical peptide according to prediction
223 by HeliQuest [33]. There are several similarities between these two self-assembling
224 peptides and the peptides identified in this study: they are both self-adjuvanting,
225 both show low reactogenicity, and they are all amphipathic peptides, suggesting
226 they might also share similar mechanisms that demand further studies.
227 In conclusion, the fusion with an amphipathic helical peptide provides a novel
228 mechanism for stimulating immunity and may be applied to other antigens other
229 than GFP if the following goals can be achieved: extended protein stability, efficient
230 incorporation of heterologous proteins, and high specificity to the target cell.
231
232
233 Materials and methods

234 **Expression and purification of endotoxin free protein**

235 The pET28a vector encoding the target protein was transformed into BL21 (DE3)
236 using heat shock. The procedure for heat shock transformation is as follows: Day 1
237 at 3 p.m., plasmid of 1 ng was mixed with 50 μl of thawed competent cell,

238 BL21(DE3), and incubated on ice for 10 minutes before 42 °C heat shock for 40
239 seconds. After heat shock, the mixture was kept on ice for 1 minute before adding 1
240 ml LB and then shaken at 220 rpm at 37 °C for 1 hour. Then the bacteria were spun
241 down at 13000 rpm for 1 minute. The bacteria pellet was re-suspended in 100 µl LB
242 and plated on LB plates with 100 µg/ml ampicillin and incubated at 37 °C. Day 2, at
243 10 a.m., there should be fewer than 100 colonies on the plate. Pick one colony and
244 inoculate the bacteris in 3 ml LB/ampicillin culture and incubated by shaking at
245 37℃/225 rpm. By 12 a.m., the 3 ml culture was transferred to 500 ml LB/ampicillin
246 media, and the growth of culture was monitored by spectrophotometer. When
247 OD600 reached 0.5-0.7, 1 mM IPTG was added into the culture to induce protein
248 expression. The culture was harvested 3 hours after protein induction. Bacteria
249 were spun down by centrifuge at 5000 rpm for 10 minutes. Supernatant were
250 removed and the pellet was kept for further processing.

251 **Protein purification**

252 The buffer for protein purification and gel filtration: 20 mM $NaPO_4$, pH 7.4, and 300
253 mM NaCl (GF buffer). For Ni-NTA resin purification: 5 mM Imidazole in GF for
254 bacteria lysis (Lysis buffer), 10 mM Imidazole in GF for wash (Wash buffer), 200 mM
255 Imidazole in GF for protein elution (Elution buffer). Bacteria pellets from 500 ml of
256 LB culture was re-suspended in 40 ml of Lysis buffer by vortex and then was lysed
257 using an ultrasonic sonicator (Misonix 3000) at 10 S on/5 S off cycles for 5 minutes.
258 The re-suspended bacteria were kept in icy water during sonication. Insoluble
259 debris was removed by centrifugation at 10000 rpm for 10 minutes using a Sorval
260 SS34 rotor at 4 °C. The supernatant containing target proteins was passed through a
261 polypropylene column containing 2 ml Ni-NTA resin from Qiagen. After the target
262 protein bound to the Ni-NTA resin, the column was washed with 10 bed volume of
263 wash buffer (20 ml). After washing, the target protein was then eluted using 5 ml

264 elution buffer. Target protein purified using Ni-NTA resin was further purified using
265 a gel filtration column from GE (HiLoad 16/600 Superdex 200 pg) on AKTA prime.

266 **Size exclusion chromatography**

267 Three programs were setup for the purification of fusion proteins in study. Program
268 30: For gel filtration purification of the fusion protein. Program 33: for the onsite
269 cleaning of HiLoad 16/600 Superdex 200 pg using 120 ml of 0.5 M NaOH. The flow
270 rate is 0.8 ml/minute. Program 34: for equilibrate the column after onsite cleaning
271 using 150 ml GF buffer. The column was washed after two protein purifications. A 5
272 ml sample loop was connected to the machine, the AKTA Prime, for holding the
273 protein sample. The sample loop was first flushed with 25 ml of GF buffer to remove
274 the residual protein from previous purification. Before loading the fusion protein
275 into the sample loop, additional 0.5 ml of GF buffer was added into the Ni-NTA
276 eluted fusion protein. The protein solution was loaded into a 5-ml syringe and
277 injected into the sample loop. The glass tubes in the corresponding fractions of
278 fusion protein eluted from the column were replaced with new tubes every time
279 before the purification. All the buffers to be used in the gel filtration experiment
280 were filtered through a 0.2-μm filter unit for sterilization and impurity. These
281 buffers were further degassed by vacuum for 10 minutes. The FPLC fractions
282 contained fusion proteins as monitored by UV280 and were collected and pooled.
283 The pooled protein solution was concentrated by a second Ni-NTA column with the
284 same bed volume as the first one. After the protein was eluted from 2nd Ni-NTA
285 column, the protein concentration was determined by BCA analysis. Two fractions
286 with highest protein concentration were pooled and dialyzed against 1 L PBS
287 overnight. After dialysis, the endotoxin contaminant was removed using
288 EndotoxinOUT™ resin from G-Bioscience. The polypropylene column was filled with
289 4 ml EndotoxinOUT™ resin and washed with 5 bed volumes of 1 % sodium

290 deoxycholate in LAL Reagent Water (LRW), 5 bed volumes of LRW and 5 bed
291 volumes of PBS/LRW before loading 1.5 ml fusion protein. After complete loading of
292 the protein, the column was placed in cold room for 1 hour for complete absorption
293 of endotoxin by resin. Protein was eluted using stepwise additions of first fraction of
294 0.5 ml and later fractions of 1 ml of PBS.

295 **LAL assay**

296 The endotoxin level was determined using PYROTELL-T LAL provided by Associate
297 of Cape Cod. Each LAL reagent supplied in lyophilized powder was first dissolved in
298 5 ml LRW and then aliquoted into small volumes and kept at -80 ^{o}C. In a typical
299 turbidity assay using PYROTELL-T, 100 μl of sample, including endotoxin standard,
300 were applied to a microplate. The reaction kinetics were measured using a victor3
301 fluorescence reader by OD405 at 37 ^{o}C. The time-lapse between each reading was
302 70 seconds and the reading was repeated 60 times. The time needed for a reaction
303 to reach a difference of 0.1 in OD405 between sample and blank was recorded and
304 compared to the endotoxin standard to determine the endotoxin unit in a sample.
305 The log of endotoxin activity was plotted against time (seconds) to reach a
306 difference of 0.1 in OD405; a logarithmic trend line is used as the standard curve.
307 The identified endotoxin activity in a protein sample was further combined with the
308 protein concentration, as determined by BCA assay, to determine specific endotoxin
309 activity, EU/mg. The upper limit of specific endotoxin activity in all the protein
310 samples was 5 EU/mg.

311

312 **Animal Immunization**

313 The C57BL/6 SPF mice used in immunization procedures were between aged 6 and
314 8 weeks and provided by BioLasco Taiwan. Without anesthetization, mouse was

315 bled from tail by clipping away 2-3 mm tail. Blood was collected using a pipette with
316 occasional massaging on the tail. About 100 μl blood was collected from each bleed.
317 Blood was left at RT for 2 hours before centrifugation at 2000 rpm for 10 minutes in
318 a microcentrifuge, and serum was collected in a microtube. Remaining lymphocytes
319 were removed by centrifugation at 2000 rpm for 10 minutes in a microcentrifuge.
320 Serum was stored at -80 ^{o}C before use in an ELISA assay. Mouse tail bleeding is
321 stopped by heated soldering iron while pressing the tail tip between fingers. For
322 primary immunization, 20 μg purified protein was injected intramuscularly in the
323 thigh of the hind limb. Blood was bled 14 days post immunization from tail and a
324 booster dose with the same amount of purified protein was injected by the same
325 procedure.

326

327 **ELISA for determining antibody titer**

328 The anti-GFP IgG titer was determined by coating GFP protein at a concentration of
329 10 μg/ml. The procedures for the ELISA assay followed the standard protocol.
330 Secondary Ab (HRP conjugated goat anti-mouse Ab) was diluted by 5000 folds in
331 blocking buffer. The coating buffer contains 0.2 M Carbonate/Bicarbonate buffer at
332 pH 9.4. The washing buffer contains 0.05% Tween 20 in 1X PBS. The blocking buffer
333 contains 1% BSA in the washing buffer, and the stop buffer contains 2M sulfuric
334 acid.

335

336 **GFP fusion protein binding assay**

337 The GFP fusion protein binding activity was tested by first plating $4x10^4$ MDCK cells
338 on one well of a 96 well plate, each sample was tested in quadruplicate. On second
339 day, 200 μg/ml of GFP fusion protein was added into the culture media and

340 incubated for 4 hours. After incubation, media was removed and washed with 200 μl
341 of PBS for three times. The amount of GFP fusion protein bound/internalized was
342 determined by a fluorometer.

343

344 **Plasma cytokine determination**

345 To detect the blood cytokine level, mice were first intramuscularly injected with
346 experimental proteins. Two hours after injection, the mice were anesthetized before
347 collecting blood through cardiac puncture with a syringe preloaded with 10 μl of
348 0.5M Na_2EDTA. The blood samples were centrifuged at 2000 rpm for 20 minutes in
349 a tabletop microcentrifuge. The plasma collected was aliquoted into 20 μl fractions
350 and snap-frozen on dry ice. The plasma cytokine level was determined by sandwich
351 ELISA with a standard from eBioscience, USA. The IL-6 level was detected using the
352 Mouse IL-6 ELISA Ready-SET-Go! (Cat#88-7064, eBioscience, USA). The MCP-1 level
353 was detected using the Mouse CCL2 (MCP-1) ELISA Ready-SET-Go! Kit [34-7391,
354 eBioscience, USA]. The detection procedures followed the manufacturer's standard
355 protocol.

356

357 **Cell apoptosis assay by flow cytometer and MTT assay**

358 MDCK cells were first plated on 6 well plates at 3x10E5 cells/well. Twenty-four
359 hours after plating, peptides were applied to 10 μM, 30 μM, or 100 μM
360 concentrations and cells were incubated for 24 hours before harvested by trypsin
361 digestion. The suspended cells due to apoptosis were collected by centrifuging the
362 culture medium at 1000 rpm for 5 minutes. The cells collected from trypsin
363 digestion and cultured media were combined, and cells were fixed in 3 ml 70 %
364 ethanol overnight in a -20 ^{o}C freezer. After fixation, cells were washed and

365 resuspended in 1 ml PBS and stained by the SYTOX AADvanced Dead Cell Stain Kit
366 (Thermo Fisher Scientific Inc.) in the presence of 100 μg RNaseA for 30 minutes at 4
367 degree cold room before analysis by flow cytometry (Calibur BD). The sub-G1
368 fraction was calculated and designated as apoptotic cells. For MTT assay, MDCK cells
369 were plated at 1x10E4 cell/well. Twenty-four hours after plating, peptide was
370 added to reach a concentration of 10 μM, 30 μM, or 100 μM and cells were incubated
371 for 24 hours and media removed and replaced with 50 μl serum free media and 50
372 μl MTT solution. After incubation at 37 ^{o}C for 3 hours, 150 MTT solvent was added
373 and the plate was shaked for 15 minutes and then read the absorbance at OD570.

374

375 **Transmission electronic microscope**

376 Madin-Darby canine kidney (MDCK) cells were seeded on ACLAR EMBEDDING film
377 in a 6-well plate at a density of $3x10^5$ cells per well. After overnight culturing, part of
378 the media were removed to leave 0.5 ml of culture media before adding 50 μl of 10
379 nm gold nanoparticles conjugated with AH2 peptide. The peptide density of AH2
380 conjugated 10 nm gold nanoparticle used in this assay was $4.78x10^{12}$/ml. After 4
381 hours of incubation, cells were washed in serum-free culture media at room
382 temperature and fixed directly or cultured for an additional 20 hrs before fixation.
383 The fixation procedure involved covering the film in 2.5% glutaraldehyde, 0.1%
384 tannic acid, 0.1M cacodylate buffer, pH 7.2 at room temperature for 30 minutes.
385 Then cells were washed in 0.1M cacodylate buffer pH 7.2, 0.2M sucrose, 0.1% $CaCl_2$
386 for 5 minutes at room temperature. Afterward, cells were post-fixed in 1%
387 OsO_4/0.1M cacodylate buffer, pH 7.2 at room temperature for 30 minutes. Then cells
388 were washed with ddH_2O three times for 5 minutes each at room temperature. Cells
389 were further stained with 1% uranyl acetate at room temperature for 30 minutes
390 before being washed in ddH_2O for 3 times. Cell were then dehydrated and

391 embedded in EPON by polymerizing at 60 ^{o}C for 24 hours. Embedded cells were
392 then sectioned for observation under a transmission electronic microscope.
393
394
395
396

397 **Figures**

398

399 Figure 1

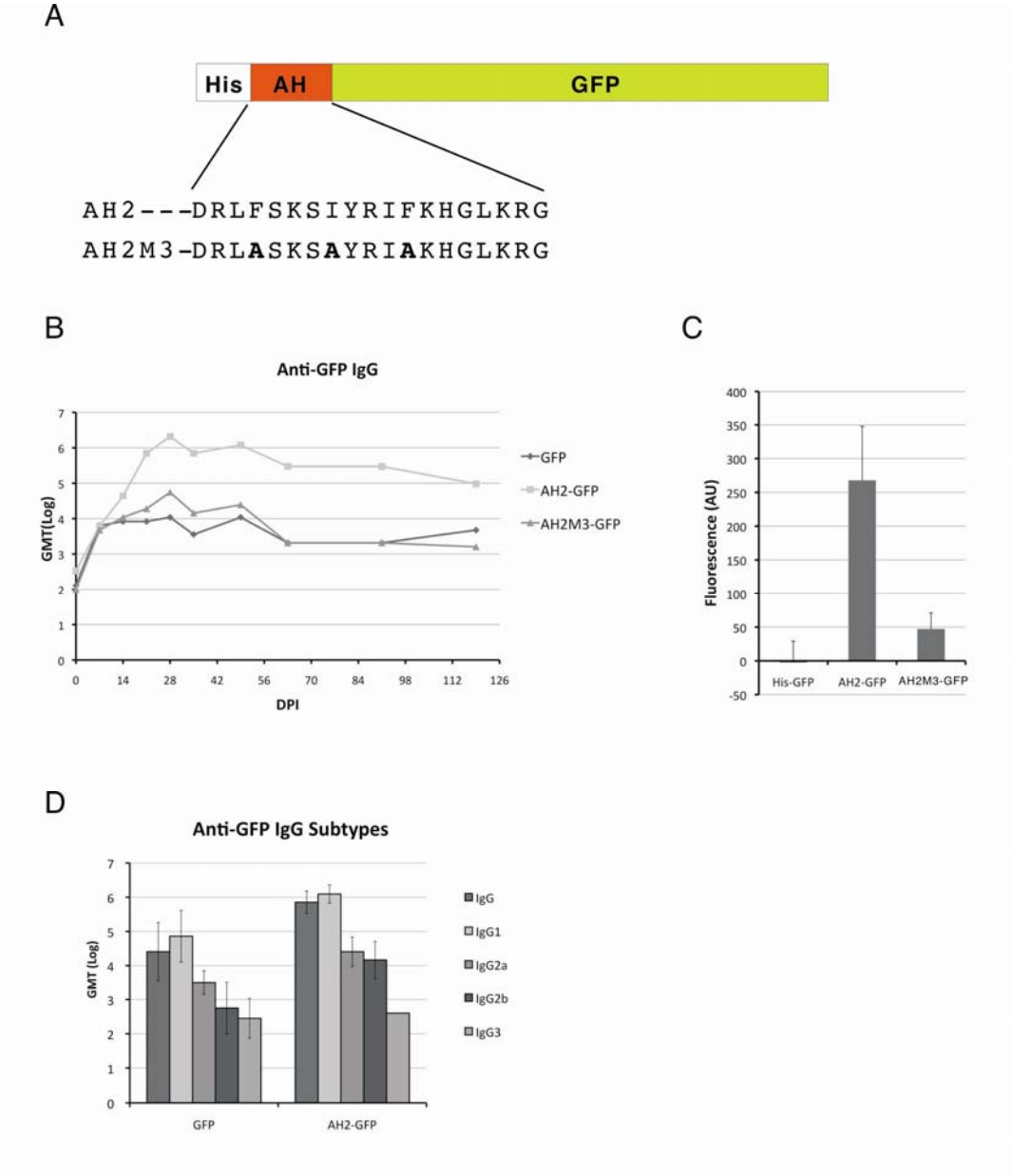

400

401 Figure 1. The effect of AH peptide mediated recombinant protein antigenicity
402 enhancement. (A) The design of the AH fusion protein was shown. The AH peptide
403 from the M2 protein of influenza virus strain A/TW/3355/97 H1N1 (AH2) was
404 inserted between His-Tag and GFP. The amino-acid sequence of the AH2 peptide

405 and its membrane binding mutant, AH2M3, were shown. (B) The change of anti-GFP
406 IgG titers was determined by ELISA and followed for 4 months. Mice were
407 immunized twice with 20 μg each of His-GFP, AH2-GFP, or AH2M3-GFP at days 0
408 and 14 by intramuscular injection. Sera for ELISA assay were collected every 7 days
409 at first month, every 2 weeks up to second month and monthly up to fourth month.
410 The anti-GFP IgG geometric mean titer was shown as GMT (Log) (N=5). (C) The
411 membrane binding activity of fusion proteins was measured by incubating the
412 fusion proteins with cultured MDCK cells for 4 hours and then washing with PBS for
413 quantification under a fluorometer. (D) The anti-GFP IgG subtypes of sera collected
414 at day 28 after the primary dose of His-GFP or AH2-GFP were determined. HRP-
415 conjugated goat anti-mouse IgG1, goat anti-mouse IgG2a, goat anti-mouse IgG2b,
416 and goat anti-mouse IgG3 secondary antibodies were used in the ELISA assay.

417

418 Figure 2

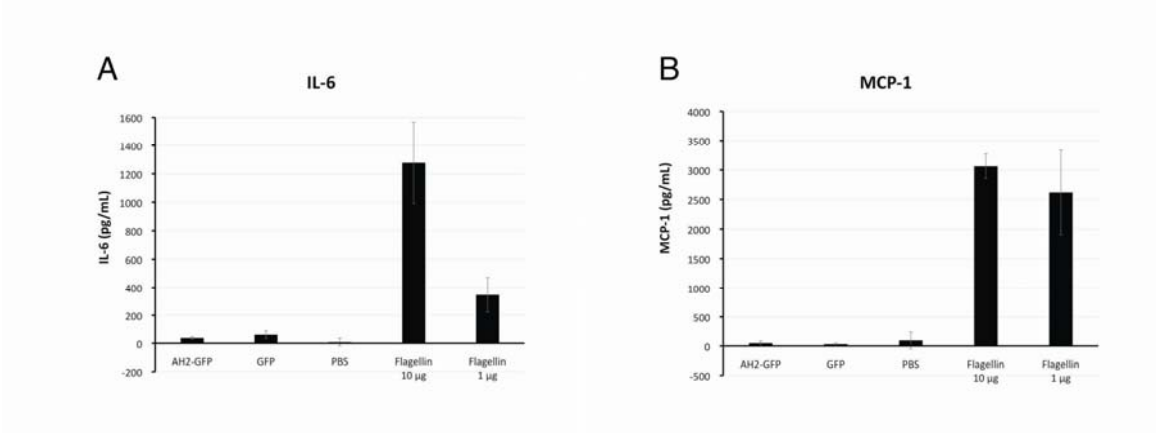

419

420 Figure 2. Detection of inflammatory cytokine levels after antigen immunization.
421 Mice were injected with either PBS, His-GFP, AH2-GFP, 10 μg flagellin or 1 μg
422 flagellin and plasma was collected 2 hours post immunization for detection of A) IL-
423 6 and B) MCP-1 by sandwich ELISA. (N=5).

424 Figure 3

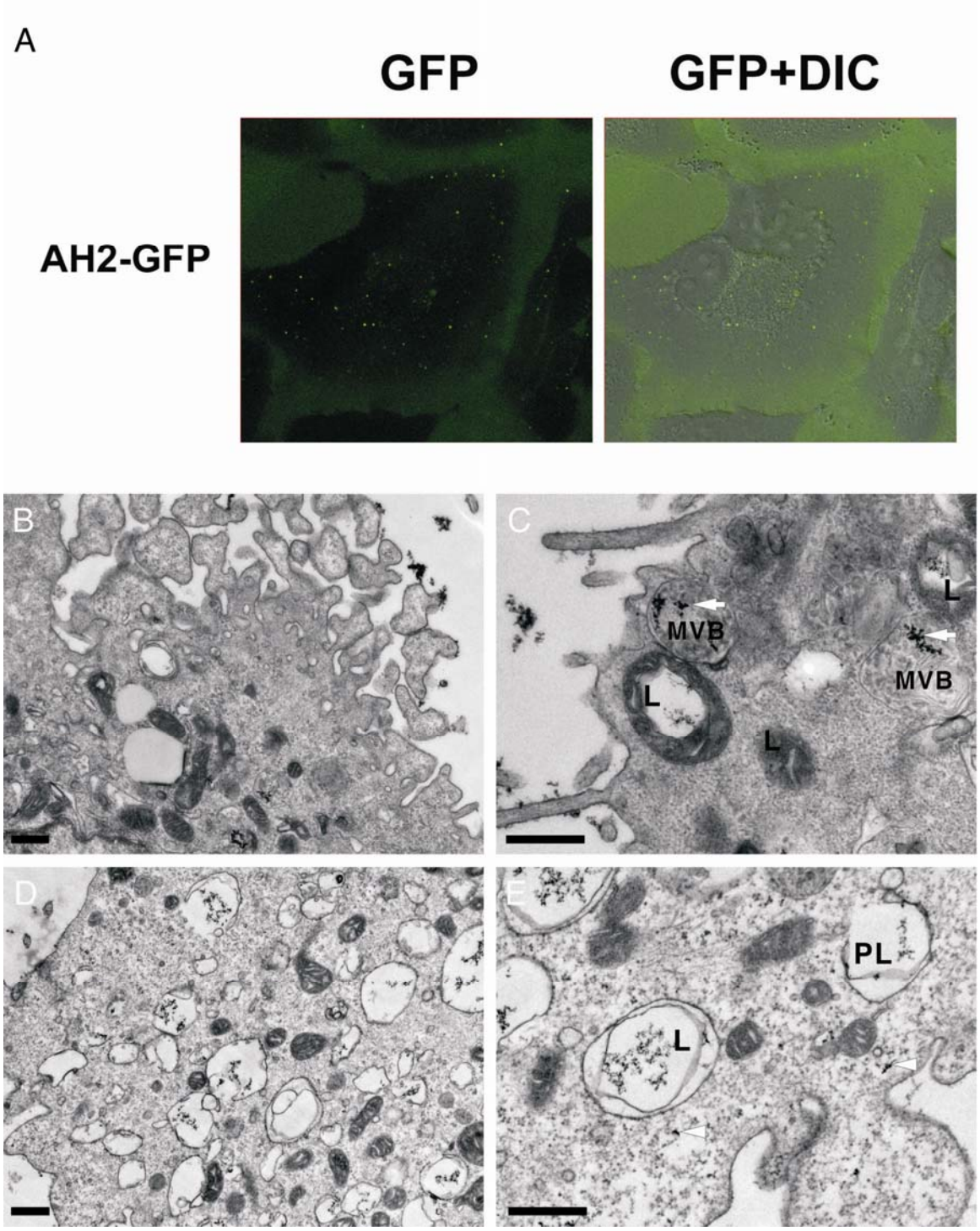

425

426 Figure 3. The binding and transportation of AH2-GFP and AH2-G-NP into cytoplasm

427 were examined under a confocal fluorescence microscope or transmission

428 electronic microscope (TEM). (A) Purified AH2-GFP fusion protein was incubated
429 with cultured MDCK cells and non-binding protein was washed away after 4 hours
430 of incubation. The location of internalized AH2-GFP was traced by confocal
431 fluorescence microscopy. The transportation of AH2 peptide conjugated gold
432 nanoparticles (AH2-G-NP) was traced by TEM. The MDCK cell was incubated with
433 AH2-G-NP for either (B-C) 4 hours or (D-E) 4+20 hours before it was fixed and
434 embedded for TEM imaging. The arrow points to the internalized AH2-G-NP in the
435 lysosome (L) or permeabilized lysosome (PL) or the multivesicular body (MVB). The
436 arrowheads pointed to the positions of released AH2-G-NP in cytoplasm. The length
437 of the scale bar is 500 nm.

438 Figure 4

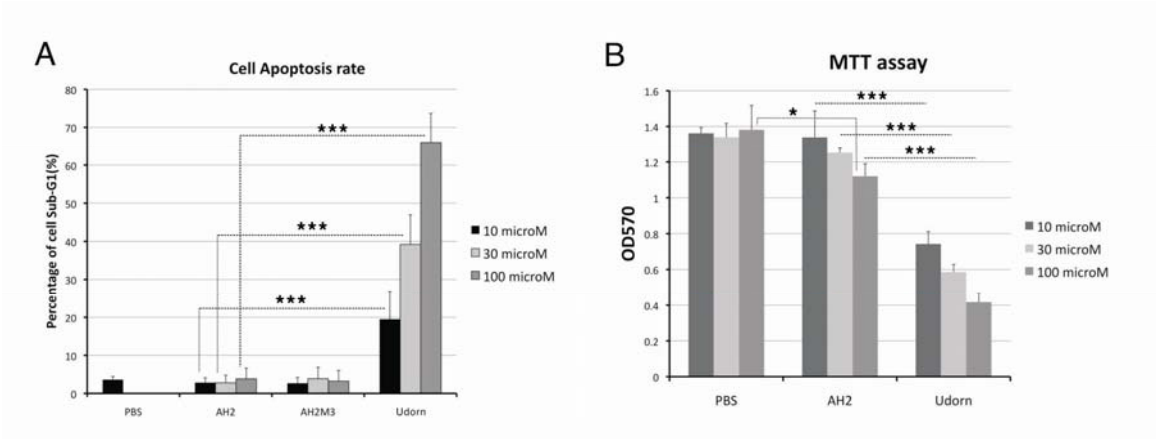

439

440 Figure 4. Evaluating the cytotoxic effects of amphipathic helical peptides by flow
441 cytometry and MTT assays. (A) The percentage of cells in apoptosis after being
442 exposed to the AH peptide was measured by flow cytometry. MDCK cells were
443 incubated with 10 microM, 30 microM or 100 microM of synthetic peptides for 24
444 hrs, and then the cells were harvested for detecting apoptotic cells using nuclei
445 staining. (B) The viability of MDCK cells after being incubated with synthetic
446 peptides for 24 hours was measured by the MTT assay. The AH2 peptide or Udorn

447 peptide was added into the culture media in increasing concentrations of 10
448 microM, 30 microM or 100 microM. (*** P≤0.001, * P≤0.05)

449

450 Figure 5

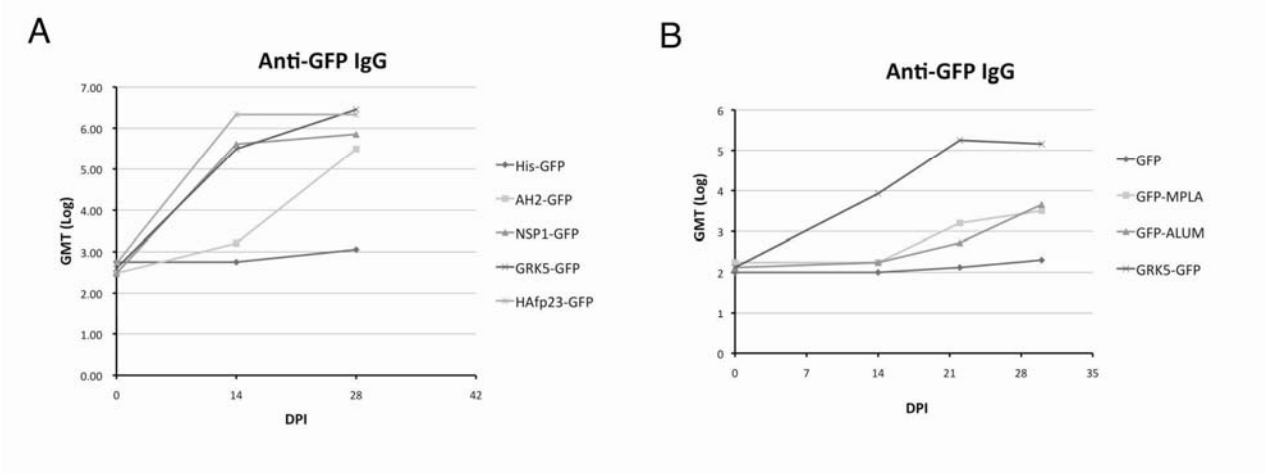

451

452 Figure 5. The evaluation of different amphipathic helical peptides in enhancing GFP
453 antigenicity and the comparison with other adjuvants. (A) The AH peptides from M2
454 protein of H1N1 influenza virus (AH2-GFP), Semliki Forest virus replicase nsP1
455 (NSP1-GFP), G-protein coupled kinase 5 (GRK5-GFP), and the fusion hairpin peptide
456 of hemaglutinin (HAfp23-GFP) were fused with GFP, and the fusion proteins were
457 purified and used for mouse immunization in a two doses protocol. The anti-GFP IgG
458 titer was determined from sera collected 14 days after immunization. (B) The
459 comparison of GFP antigenicity boosting by either GRK5 peptide (GRK5-GFP), alum
460 salt (GFP-ALUM), or MPLA (GFP-MPLA) in a two-dose immunization protocol. The
461 anti-GFP IgG titer was determined using ELISA. (N=5)

462

463

464 References

465 1. FDA. Regulatory Considerations in the Safety Assessment of Adjuvants and
466 Adjuvanted Preventive Vaccines
467 2. Almeida, P.F. Membrane-active peptides: binding, translocation, and flux in
468 lipid vesicles. *Biochim Biophys Acta* **2014**, *1838*, 2216-2227,
469 doi:10.1016/j.bbamem.2014.04.014 [doi].
470 3. Pinto, L.H.; Lamb, R.A. The M2 proton channels of influenza A and B viruses. *J*
471 *Biol Chem* **2006**, *281*, 8997-9000, doi:10.1074/jbc.R500020200 [doi].
472 4. Rossman, J.S.; Jing, X.; Leser, G.P.; Lamb, R.A. Influenza virus M2 protein
473 mediates ESCRT-independent membrane scission. *Cell* **2010**, *142*, 902-913,
474 doi:10.1016/j.cell.2010.08.029 [doi].
475 5. Martyna, A.; Bahsoun, B.; Madsen, J.J.; Jackson, F.S.J.S.; Badham, M.D.; Voth,
476 G.A.; Rossman, J.S. Cholesterol Alters the Orientation and Activity of the
477 Influenza Virus M2 Amphipathic Helix in the Membrane. *J Phys Chem B* **2020**,
478 *124*, 6738-6747, doi:10.1021/acs.jpcb.0c03331 [doi].
479 6. Elkins, M.R.; Williams, J.K.; Gelenter, M.D.; Dai, P.; Kwon, B.; Sergeyev, I.V.;
480 Pentelute, B.L.; Hong, M. Cholesterol-binding site of the influenza M2 protein
481 in lipid bilayers from solid-state NMR. *Proc Natl Acad Sci U S A* **2017**, *114*,
482 12946-12951, doi:10.1073/pnas.1715127114 [doi].
483 7. Pan, J.; Dalzini, A.; Song, L. Cholesterol and phosphatidylethanolamine lipids
484 exert opposite effects on membrane modulations caused by the M2
485 amphipathic helix. *Biochim Biophys Acta Biomembr* **2018**, *1861*, 201-209,
486 doi:10.1016/j.bbamem.2018.07.013 [doi].
487 8. Tossi, A.; Sandri, L.; Giangaspero, A. Amphipathic, alpha-helical antimicrobial
488 peptides. *Peptide Science* **2000**, *55*, 4-30, doi:10.1002/1097-
489 0282(2000)55:1<4::aid-bip30>3.0.co;2-m.
490 9. Möbius, W.; van Donselaar, E.; Ohno-Iwashita, Y.; Shimada, Y.; Heijnen, H.F.;
491 Slot, J.W.; Geuze, H.J. Recycling compartments and the internal vesicles of
492 multivesicular bodies harbor most of the cholesterol found in the endocytic
493 pathway. *Traffic* **2003**, *4*, 222-231, doi:10.1034/j.1600-0854.2003.00072.x
494 [doi].
495 10. Welsby, I.; Detienne, S.; N'Kuli, F.; Thomas, S.; Wouters, S.; Bechtold, V.; De
496 Wit, D.; Gineste, R.; Reinheckel, T.; Elouahabi, A.; et al. Lysosome-Dependent
497 Activation of Human Dendritic Cells by the Vaccine Adjuvant QS-21. *Front*
498 *Immunol* **2017**, *7*, 663, doi:10.3389/fimmu.2016.00663 [doi].
499 11. Brojatsch, J.; Lima, H.; Kar, A.K.; Jacobson, L.S.; Muehlbauer, S.M.; Chandran,
500 K.; Diaz-Griffero, F. A proteolytic cascade controls lysosome rupture and
501 necrotic cell death mediated by lysosome-destabilizing adjuvants. *PLoS One*
502 **2014**, *9*, e95032, doi:10.1371/journal.pone.0095032 [doi].
503 12. Jacobson, L.S.; Lima, H., Jr.; Goldberg, M.F.; Gocheva, V.; Tsiperson, V.;
504 Sutterwala, F.S.; Joyce, J.A.; Gapp, B.V.; Blomen, V.A.; Chandran, K.; et al.
505 Cathepsin-mediated necrosis controls the adaptive immune response by Th2
506 (T helper type 2)-associated adjuvants. *J Biol Chem* **2013**, *288*, 7481-7491,
507 doi:10.1074/jbc.M112.400655 [doi].

508 13. Ito, T.; Inouye, K.; Fujimaki, H.; Tohyama, C.; Nohara, K. Mechanism of TCDD-
509 induced suppression of antibody production: effect on T cell-derived
510 cytokine production in the primary immune reaction of mice. *Toxicol Sci*
511 **2002**, *70*, 46-54, doi:10.1093/toxsci/70.1.46 [doi].
512 14. Duewell, P.; Kisser, U.; Heckelsmiller, K.; Hoves, S.; Stoitzner, P.; Koernig, S.;
513 Morelli, A.B.; Clausen, B.E.; Dauer, M.; Eigler, A.; et al. ISCOMATRIX adjuvant
514 combines immune activation with antigen delivery to dendritic cells in vivo
515 leading to effective cross-priming of CD8+ T cells. *J Immunol* **2011**, *187*, 55-
516 63, doi:10.4049/jimmunol.1004114 [doi].
517 15. Baz Morelli, A.; Becher, D.; Koernig, S.; Silva, A.; Drane, D.; Maraskovsky, E.
518 ISCOMATRIX: a novel adjuvant for use in prophylactic and therapeutic
519 vaccines against infectious diseases. *J Med Microbiol* **2012**, *61*, 935-943,
520 doi:10.1099/jmm.0.040857-0 [doi].
521 16. Wilson, N.S.; Yang, B.; Morelli, A.B.; Koernig, S.; Yang, A.; Loeser, S.; Airey, D.;
522 Provan, L.; Hass, P.; Braley, H.; et al. ISCOMATRIX vaccines mediate CD8+ T-
523 cell cross-priming by a MyD88-dependent signaling pathway. *Immunol Cell*
524 *Biol* **2012**, *90*, 540-552, doi:10.1038/icb.2011.71 [doi].
525 17. Kramer, R.M.; Archer, M.C.; Orr, M.T.; Dubois Cauwelaert, N.; Beebe, E.A.;
526 Huang, P.D.; Dowling, Q.M.; Schwartz, A.M.; Fedor, D.M.; Vedvick, T.S.; et al.
527 Development of a thermostable nanoemulsion adjuvanted vaccine against
528 tuberculosis using a design-of-experiments approach. *Int J Nanomedicine*
529 **2018**, *13*, 3689-3711, doi:10.2147/IJN.S159839 [doi].
530 18. Gomez, M.; Archer, M.; Barona, D.; Wang, H.; Ordoubadi, M.; Bin Karim, S.;
531 Carrigy, N.B.; Wang, Z.; McCollum, J.; Press, C.; et al. Microparticle
532 encapsulation of a tuberculosis subunit vaccine candidate containing a
533 nanoemulsion adjuvant via spray drying. *Eur J Pharm Biopharm* **2021**, *163*,
534 23-37, doi:10.1016/j.ejpb.2021.03.007 [doi].
535 19. Kan, M.-C. The thermostability of a VADEX-Pro based protein nanoparticle.
536 *bioRxiv* **2023**, doi:10.1101/2023.02.15.528623.
537 20. Wong, T.-T.; Liou, G.-G.; Kan, M.-C. A Thermal-Stable Protein Nanoparticle
538 That Stimulates Long Lasting Humoral Immune Response. *Vaccines* **2023**, *11*,
539 426.
540 21. Thiyagarajan, M.M.; Stracquatanio, R.P.; Pronin, A.N.; Evanko, D.S.; Benovic,
541 J.L.; Wedegaertner, P.B. A predicted amphipathic helix mediates plasma
542 membrane localization of GRK5. *J Biol Chem* **2004**, *279*, 17989-17995,
543 doi:10.1074/jbc.M310738200 [doi.
544 22. Ding, B.; Glukhova, A.; Sobczyk-Kojiro, K.; Mosberg, H.I.; Tesmer, J.J.; Chen, Z.
545 Unveiling the membrane-binding properties of N-terminal and C-terminal
546 regions of G protein-coupled receptor kinase 5 by combined optical
547 spectroscopies. *Langmuir* **2014**, *30*, 823-831, doi:10.1021/la404055a [doi].
548 23. Lampio, A.; Kilpeläinen, I.; Pesonen, S.; Karhi, K.; Auvinen, P.; Somerharju, P.;
549 Kääriäinen, L. Membrane binding mechanism of an RNA virus-capping
550 enzyme. *J Biol Chem* **2000**, *275*, 37853-37859, doi:10.1074/jbc.M004865200
551 [doi].
552 24. Spuul, P.; Salonen, A.; Merits, A.; Jokitalo, E.; Kääriäinen, L.; Ahola, T. Role of
553 the amphipathic peptide of Semliki forest virus replicase protein nsP1 in

554 membrane association and virus replication. *J Virol* **2007**, *81*, 872-883,
555 doi:10.1128/JVI.01785-06 [doi].
556 25. Zhang, K.; Law, Y.S.; Law, M.C.Y.; Tan, Y.B.; Wirawan, M.; Luo, D. Structural
557 insights into viral RNA capping and plasma membrane targeting by
558 Chikungunya virus nonstructural protein 1. *Cell Host Microbe* **2021**, *29*, 757-
559 764 e753, doi:10.1016/j.chom.2021.02.018 [doi].
560 26. Smrt, S.T.; Draney, A.W.; Lorieau, J.L. The influenza hemagglutinin fusion
561 domain is an amphipathic helical hairpin that functions by inducing
562 membrane curvature. *J Biol Chem* **2015**, *290*, 228-238,
563 doi:10.1074/jbc.M114.611657 [doi].
564 27. Cruz-Reséndiz, A.; Zepeda-Cervantes, J.; Sampieri, A.; Bastián-Eugenio, C.;
565 Acero, G.; Sánchez-Betancourt, J.I.; Gevorkian, G.; Vaca, L. A self-aggregating
566 peptide: implications for the development of thermostable vaccine
567 candidates. *BMC Biotechnol* **2020**, *20*, 1, doi:10.1186/s12896-019-0592-9
568 [doi].
569 28. Rudra, J.S.; Tian, Y.F.; Jung, J.P.; Collier, J.H. A self-assembling peptide acting as
570 an immune adjuvant. *Proc Natl Acad Sci U S A* **2010**, *107*, 622-627,
571 doi:10.1073/pnas.0912124107 [doi].
572 29. Rudra, J.S.; Mishra, S.; Chong, A.S.; Mitchell, R.A.; Nardin, E.H.; Nussenzweig,
573 V.; Collier, J.H. Self-assembled peptide nanofibers raising durable antibody
574 responses against a malaria epitope. *Biomaterials* **2012**, *33*, 6476-6484,
575 doi:10.1016/j.biomaterials.2012.05.041 [doi].
576 30. Votaw, N.L.; Collier, L.; Curvino, E.J.; Wu, Y.; Fries, C.N.; Ojeda, M.T.; Collier,
577 J.H. Randomized peptide assemblies for enhancing immune responses to
578 nanomaterials. *Biomaterials* **2012**, *273*, 120825,
579 doi:10.1016/j.biomaterials.2021.120825 [doi].
580 31. Wu, Y.; Norberg, P.K.; Reap, E.A.; Congdon, K.L.; Fries, C.N.; Kelly, S.H.;
581 Sampson, J.H.; Conticello, V.P.; Collier, J.H. A Supramolecular Vaccine Platform
582 Based on Œ±-Helical Peptide Nanofibers. *ACS Biomater Sci Eng* **2017**, *3*,
583 3128-3132, doi:10.1021/acsbiomaterials.7b00561 [doi].
584 32. Wu, Y.; Kelly, S.H.; Sanchez-Perez, L.; Sampson, J.H.; Collier, J.H. Comparative
585 study of α-helical and β-sheet self-assembled peptide nanofiber vaccine
586 platforms: influence of integrated T-cell epitopes. *Biomater Sci* **2020**, *8*,
587 3522-3535, doi:10.1039/d0bm00521e [doi].
588 33. Gautier, R.; Douguet, D.; Antonny, B.; Drin, G. HELIQUEST: a web server to
589 screen sequences with specific alpha-helical properties. *Bioinformatics* **2008**,
590 *24*, 2101-2102, doi:10.1093/bioinformatics/btn392 [doi].
591
592
593